THE PHOTOELECTRIC HEATING MECHANISM FOR VERY SMALL GRAPHITIC GRAINS AND POLYCYCLIC AROMATIC HYDROCARBONS

E. L. O. BAKES

Princeton University Observatory, Peyton Hall, Princeton, NJ 08544

AND

A. G. G. M. TIELENS

NASA Ames Research Center, MS 245-3, Moffet Field, CA 94035

ABSTRACT

We have theoretically modeled the gas heating associated with the photoelectric ejection of electrons from a size distribution of interstellar carbon grains which extends into the molecular domain. We have considered a wide range of physical conditions for the interstellar gas ($1 < G_0 < 10^5$, with G_0 being the intensity of the incident far-UV field in units of the Habing interstellar radiation field; $2.5 \times 10^{-3} < n_e < 75$ cm^{-3}, with n_e being the electron density; $10 < T < 10,000$ K, with T being the gas temperature). The results show that about half of the heating is due to grains less than 1500 C atoms (<15 Å). The other half originates in somewhat larger grains (1500–4.5×10^5 C atoms; $15 < a < 100$ Å). While grains larger than this do absorb about half of the available far-UV photons, they do not contribute appreciably to the gas heating. This strong dependence of gas heating on size results from the decrease in yield and from the increased grain charge (hence larger Coulomb losses) with increasing grain size.

We have determined the net photoelectric heating rate and evaluated a simple analytical expression for the heating efficiency, dependent only on G_0, T, and n_e. This expression is accurate to 3% over the whole parameter range and is valid up to gas temperatures of 10^4 K, at which point the dominant gas-dust heat exchange mechanism becomes the recombination of electrons with grains rather than photoelectric ejection. The calculated heating efficiency for neutral grains is in good agreement with that derived from observations of the diffuse interstellar clouds. Our results also agree well with the FIRAS observations on *COBE*. Finally, our photoelectric heating efficiency is compared to previous studies.

Subject headings: dust, extinction — ISM: general — ISM: molecules — molecular processes

1. INTRODUCTION

The structure of the interstellar medium depends to a large extent on the heating and cooling sources of the interstellar gas (Goldsmith, Habing, & Field 1969; de Jong 1977; McKee & Ostriker 1977; Draine 1978; Ferrière, Zweibel, & Shull 1988). The photoelectric effect on interstellar dust grains is thought to be the dominant heating source of the neutral atomic interstellar gas and may play an important role in the warm intercloud medium as well. Absorption of a far-UltraViolet (FUV) photon by a dust grain may lead to the ejection of an electron which carries some of the photon energy away in the form of kinetic energy. This excess kinetic energy then leads to heating of the gas. Despite its importance, the photoelectric effect on interstellar dust grains is not well understood on a fundamental level. Many studies rely, therefore, on a semiempirical model based upon the measured cooling rate of the interstellar gas in a few lines of sight (see de Jong 1977).

The cooling of interstellar gas is difficult to observe directly in the general interstellar medium. However, over the last decade, observations of the dominant cooling lines—the far-IR (FIR) atomic fine structure lines of [C II] and [O I]—have become feasible for neutral atomic regions close to O and B stars. Study of such UV-illuminated regions—commonly called photodissociation regions (hereafter PDRs, generally associated with H II regions, planetary nebulae, and normal and active galactic nuclei)—has the added advantage that because of energetic considerations, UV photons have to be the dominant heating source of the gas. Indeed, fine sructure lines of these regions show that about 0.001–0.01 of the available UV photon energy is converted into gas heating (Hollenbach 1989). Hence, the interstellar gas has to be able to couple well to the stellar photons. Direct coupling of nonionizing photons to neutral gas is, however, difficult due to its low gas opacity. Instead, most of these photons will be absorbed by the dust, and most of the absorbed energy will be reradiated in the near-IR and FIR. This makes the photoelectric effect, of course, an attractive heating source for such regions, and quite detailed models have been developed for PDRs based upon these premises (Tielens & Hollenbach 1985; Sternberg & Dalgarno 1989; Wolfire, Tielens, & Hollenbach 1990; Hollenbach, Takahashi, & Tielens 1991).

In recent years, it has become abundantly clear that the size distribution of carbonaceous interstellar grains extends well into the molecular domain (i.e., down to 5 Å or $\simeq 50$ C atoms; for a review see Allamandola, Tielens, & Barker 1989). The evidence for such small species is based upon IR observations of reflection nebulae and H II regions far from the illuminating star. The strong near-IR emission observed in such regions—mainly in the form of emission features at 3.3, 6.2, 7.7, and 11.3 μm—implies much higher dust temperatures than attainable in radiative equilibrium with the stellar light. The IR emission is therefore attributed to small species temporarily heated to a high temperature through the absorption of a single UV photon (Sellgren 1984). Spectroscopically, the observed emission features are characteristic of polycyclic aromatic hydrocarbon (PAH) materials. Combination of the spectroscopic

and energetic argument leads to the identification of PAH molecules with $\simeq 50$ C atoms as an important component of the interstellar gas. Derived abundances of these species are of the order of 10^{-7}, making them the most abundant interstellar molecules after H_2 and CO. Such small species will be particularly efficient in heating the gas photoelectrically (Watson 1972; Léger & d'Hendecourt 1987).

In view of these new developments, we reexamine the photoelectric heating of the interstellar gas using an "ab initio" approach. In this paper, we investigate the photoelectric heating of the interstellar gas by a size distribution of carbon grains which extends down to molecular sizes. We also allow for multiple ionization stages of the grains. In § 2 we develop a model for the photoelectric effect. In § 3, we present our results of a study of a wide range of parameter space. In § 4, these results are combined into a simple analytical function which describes the photoelectric heating efficiency as a function of the physical parameters of a region. The derived photoelectric heating rates are compared to observations of the heating of the interstellar gas in § 5. In § 6, we discuss the effects of recombination cooling on the overall gas-dust heat exchange. Finally, in § 7, we summarize the results of our model.

2. METHOD

The photoelectric ejection of electrons from dust grains is widely accepted as being an important source of heating for the ISM (Watson 1972; de Jong 1977; Tielens & Hollenbach 1985). When small grains of radius ≤ 100 Å absorb a FUV photon, an ionization process leading to the ejection of an electron may occur. A fraction of the absorbed UV photon energy is dissipated by inelastic collisions of the excited electron with the carbon atoms in the grain as it scatters through the grain material on its way to the surface. Some is expended in overcoming the work function of a grain, and part is required to overcome the Coulomb barrier set up by positive charge due to any previous electron ejections. The electron will emerge from the grain with kinetic energy, and this will be converted to thermal energy of the gas via inelastic collisions. The net photoelectric heating rate $H(N_C, Z)$ per grain composed of N_C carbon atoms and possessing charge Z is given by

$$H(N_C, Z) = W\pi \int_{\nu_Z}^{\nu_H} \sigma_{abs}(N_C) Y_{ion}(N_C, IP_z)$$
$$\times B_\nu(\nu, T_{eff}) g(N_C, IP_z) d\nu , \quad (1)$$

where W is the FUV dilution factor of the incident blackbody radiation field at temperature T_{eff} such that

$$W = \frac{1.6 \times 10^{-3} G_0}{\sigma T_{eff}^4 F_{FUV}} ,$$

where G_0 is the FUV flux normalized to the Habing field for the solar neighborhood and F_{FUV} is the fraction of FUV flux contained in the spectrum considered. The photoelectric heating rate thus depends on the photon absorption cross section, σ_{abs}, the photoelectric ionization yield, Y_{ion}, and the kinetic energy partition function, $g(N_C, IP_z)$. The last parameter defines the fraction of photon energy carried away as kinetic energy by the photoejected electron. The term ν_H is the Lyman frequency, ν_z is the frequency corresponding to the ionization potential IP_z of a grain of charge Z and B_ν is the Planck function.

For a size distribution of grains $n(N_C)dN_C$, where $n(N_C)$ is the number density of grains with carbon atoms in the range N_C to

$(N_C + dN_C)$, the photoelectric heating rate is

$$\Gamma_{pe} = \int_{N_-}^{N_+} \sum_Z H(N_C, Z) f(N_C, Z) n(N_C) dN_C , \quad (2)$$

where $f(N_C, Z)$ is the probability of finding a grain composed of N_C carbon atoms at a certain charge Z. The summation over Z for each value of N_C is taken over all allowable ionization states and the range over which N_C is integrated runs from the smallest number of carbon atoms N_- to the largest N_+.

The recombination of charged particles with a grain containing N_C carbon atoms removes energy from the gas at a rate $C(N_C, Z)$ and thus the effective heating rate $\Psi(N_C)$ may be summarized as

$$\Psi(N_C) = \sum_Z [H(N_C, Z) - C(N_C, Z)] f(N_C, Z) n(N_C) N_C . \quad (3)$$

For the entire grain population from N_- to N_+, the net heating rate is given by Γ_{net}, where

$$\Gamma_{net} = \int_{N_-}^{N_+} \Psi(N_C) d\ln(N_C) . \quad (4)$$

The photoelectric heating rate depends on the average charge state of the grain through the fraction of the UV photon energy carried away by the electron. Furthermore, the average charge state determines the grain ionization potential and, hence, the photon energy required to eject another electron. Previous studies have limited themselves to a study of a typical grain with an average charge, while this analysis investigates a distribution of grain radii and all allowed charge states for each size.

In the following sections, derivations are made of the grain charge distribution resulting from the balance of the photoelectric effect with ion/electron-grain recombination. This allows the derivation of the gas-grain photoelectric heating rate and the cooling associated with the recombination of grains and charged particles.

2.1. Grain Charge

In our analysis of the photoelectric efficiency, we will follow the elegant study of Draine & Sutin (1987) for grain charging in the ISM. While they mainly concentrated on pure collisional charging, their analysis can be extended to include grain charging via the photoelectric effect. The grain charge is balanced between the recombination of positive ions with the grain plus the ejection of electrons from the grain via the photoelectric effect and the recombination of electrons with the grain.

The probability of finding a grain at charge Ze is defined as $f(Z)$. Considering only collisions of the grains with electrons and ions of charge $Z = 1$, detailed balance yields

$$f(Z)[J_{pe}(Z) + J_{ion}(Z)] = f(Z + 1) J_e(Z + 1) , \quad (5)$$

where J_{pe} is the rate of photoelectron emission, and J_{ion} and J_e are the accretion rate of ions and electrons, respectively.

To obtain $f(Z)$, we successively apply the following equations

$$f(Z > 0) = f(0) \prod_{Z'=1}^{Z} \left[\frac{J_{pe}(Z' - 1) + J_{ion}(Z' - 1)}{J_e(Z')} \right] , \quad (6)$$

$$f(Z < 0) = f(0) \prod_{Z'=Z}^{-1} \left[\frac{J_e(Z' + 1)}{J_{pe}(Z') + J_{ion}(Z')} \right] , \quad (7)$$

and the multiplicative constant $f(0)$ (the fraction of neutral grains) is determined via the normalization condition

$$\sum_{-\infty}^{\infty} f(Z) = 1 . \tag{8}$$

While J_{ion} and J_e are relatively simple to evaluate, J_{pe} requires more detailed considerations. In the case of a PDR, J_{pe} is usually much greater than J_{ion}, and we will ignore the ion accretion rate in the remainder of this paper when we formulate simple approximations concerning ionization rates.

2.1.1. *Collisional Charging Rates*

The general rate, J_i, of collisions of a singly charged particle of type i with number density n_i, mass m_i, and sticking coefficient s_i, with a grain surface, is given by

$$J_i(Z) = n_i s_i \left(\frac{8kT}{\pi m_i}\right)^{1/2} \pi a^2 \tilde{J}\left(\tau = \frac{akT}{q_i^2}, v = \frac{Ze}{q_i}\right), \tag{9}$$

where a is the grain radius, T is the gas temperature, τ is the "reduced temperature," q_i is the charge of the approaching particle, and $\tilde{J}$ allows for a velocity dependent collision cross section, including the effect of the image charge (Draine & Sutin 1987). The sticking coefficient s_i of a charged particle to a grain is taken as unity for both electrons and ions. Although we recognize that the electron sticking coefficient may be very small when the electron affinity of the grain is less than 1 eV (i.e., $N_C \lesssim 25$–50 carbon atoms; see Allamandola, Tielens & Barker 1989), for simplicity, we have adopted a value of unity, independent of grain size. Generally, even for the smallest grains, the electron affinity is greater than 1 eV (§ 2.1.3). The ion sticking coefficient s_{ion} is likely to be unity (see Draine & Sutin 1987). The function $\tilde{J}$ depends on the respective charges of the grain and the approaching particle, which may be neutral, negative, or positive. If the grain is neutral ($v = 0$), then

$$\tilde{J}(\tau, v = 0) = 1 + \left(\frac{\pi}{2\tau}\right)^{1/2} . \tag{10}$$

J_i contains a velocity term dependent on $T^{1/2}$. For small τ (i.e., low temperatures), J_i also contains a $\tilde{J}$ term which is dependent on $T^{-1/2}$ due to the induced dipole interaction. Hence, there is no significant temperature dependence for the recombination rate of neutral grains at low temperatures.

If v is negative, the grain and particle are of opposite charges and an attractive Coulomb potential at large distances is formed. There will be two distinct focusing stages: long-range Coulomb focusing, which enhances the capture cross section by the familiar factor $(1 - [Ze]q/akT)$, and short-range focusing by the polarization interaction (image charge), which enhances the capture cross section by a factor $(1 + [2q^2/E'a])^{1/2}$, where E' is the kinetic energy of the approaching charged particle when short-range focusing becomes effective. The slower moving the approaching charged particle is, the greater the effects of short-range focusing. Also, the smaller the grain, the greater is the attractive electrostatic force. Hence, if either of these two conditions occur for this case, an approaching charged particle is likely to be captured by the grain. Draine and Sutin obtained an analytical fit to their detailed numerical results for the short range focusing kinetic energy curve to produce the approximate result:

$$\tilde{J}(v < 0) \approx \left(1 - \frac{v}{\tau}\right)\left[1 + \left(\frac{2}{\tau - 2v}\right)^{1/2}\right], \tag{11}$$

with an accuracy of $\pm 5\%$ for $v \leq -1$ and $10^{-3} < \tau < \infty$. Considering the temperature dependence for the recombination rate, we find $J_e \propto T^{-1/2}$ when $\tau \ll 1$ and $J_e \propto T^{1/2}$ when $\tau > 1$.

As emphasized by Draine and Sutin, the most significant difference between classical grains (radius $> 0.1 \mu$m) and very small grains (radius $\ll 0.01 \mu$m) is the polarization of a dust grain by an approaching electron or ion. This image charge induces an attractive electrostatic force, and while this effect is relatively minor for classical grains and gas temperatures ~ 100 K, it is a significant factor in the charging of very small grains and grains surrounded by low-temperature gas.

For a repulsive Coulomb potential ($v > 0$), we use the approximate formula (Draine & Sutin 1987),

$$\tilde{J}(v > 0) \approx [1 + (4\tau + 3v)^{-1/2}]^2 \exp(-\theta_v/\tau), \tag{12}$$

which is accurate to within $\pm 4\%$, and where the dimensionless measure of the value of the potential maximum θ_v is given by

$$\theta_v = \frac{v}{1 + v^{-1/2}} . \tag{13}$$

For higher reduced temperature (i.e., larger kinetic energy of the approaching charged particle) or larger grain size (i.e., larger surface area over which to spread any repelling charges), the approaching charged particle is more likely to overcome the repulsion and stick to the grain.

Finally, these equations have been derived assuming spherical grains. The smallest grains are expected to be disk shaped. However, because of the dominance of Coulomb focusing effects, this leads at most to a correction factor of 0.8 (Verstraete et al. 1990) and, hence, for simplicity and generality we have chosen to ignore this difference.

2.1.2. *Photoelectric Charging*

The photoelectric ejection rate J_{pe} for a grain in the standard interstellar radiation field ($G_0 = 1$) is given by

$$J_{\text{pe}} = W\pi \int_{v_Z}^{v_H} Y_{\text{ion}} \sigma_{\text{abs}} \frac{B_v}{hv} dv \text{ electrons s}^{-1} . \tag{14}$$

For the photoelectric ionization yield Y_{ion}, measured in photoelectrons per absorbed photon, we adopt the semiempirical relation (Draine 1978) as

$$Y_{\text{ion}} = Y_\infty \left(1 - \frac{\text{IP}_z}{hv}\right) f_y(N_C), \tag{15}$$

with IP_z being the ionization potential of a grain with charge Z (§ 2.1.3). Y_∞ being a constant, and f_y being a yield enhancement factor for small grains over bulk materials (see below). Following Watson (1972) and Draine (1978), the form of this relation is chosen such that it reproduces the behavior expected for small grains—a rapid rise in photoionization yield at photon energies similar to the ionization potential followed by a roughly constant yield for higher energy photons. Watson observed that the photoemission yield of small particles is expected to be significantly larger than that of bulk materials, because for a bulk material, the photoelectron may lose all its excess energy in collisions with carbon atoms before it reaches the surface. Thus, the photoelectric yield is size dependent and our adopted values for Y_∞ and f_y reflect this, such that they reproduce measurements on bulk graphite as well as on small PAH molecules (i.e., coronene). We will thus scale Y_{ion} by the enhancement of the actual photoelectric yield, $f_y(N_C)$ of a very

small grain over that of bulk graphite. Draine (1978) has developed a simple analytical expression for this enhancement factor; viz.,

$$f_y(N_C) = \left(\frac{\zeta}{\alpha}\right)^2 \frac{(\alpha^2 - 2\alpha + 2 - 2e^{-\alpha})}{(\zeta^2 - 2\zeta + 2 - 2e^{-\zeta})}, \qquad (16)$$

where $\alpha = a/l_a + a/l_e$ and $\zeta = a/l_a$ and a is the grain radius. In the case of a disk geometry, the radius should be the minor axis of the disk. The factors l_a and l_e are the photon attenuation length and the electron escape length, respectively. Note that when $\zeta < \alpha \ll 1$,

$$f_y(N_C) = \frac{l_e + l_a}{l_e} . \qquad (17)$$

Estimates for l_e and l_a can be obtained from experimental data. A typical value of l_a is 100 Å (Pope & Swinberg 1982), and this is the value we use in this model. For l_e, a typical value is 10 Å (Hino, Sato, & Inokuchi 1976). With this choice, f_y is 11 for small PAHs. The value for l_e is uncertain and will be treated as a free parameter. Draine chose Y_∞ to reproduce the enhancement of the photoelectric yield of a small grain over bulk graphite when the grain absorbed high-energy photons, where the photoelectric yield approaches a constant value. In contrast, we normalize on the experimental data of Verstraete et al. (1990) using the photoionization cross section of coronene. With our choice of absorption cross section, this leads to $Y_\infty = 0.14$. With these parameters, the measured photoelectric cross section of small PAHs as a function of photon energy is well reproduced. Note, however, that with this choice, we formally obtain a yield greater than 1, due to the absorption cross section of coronene being somewhat higher than that of bulk graphite. Our formalism also reproduces the yield for bulk graphite at high photon energies well. However, near threshold, the yield for bulk graphite is considerably overestimated. The measured yield for bulk graphite is exceptionally small

compared to other materials (metals, for example, have 10 times higher yields). This difference is not well understood.

The FUV absorption cross section σ_{abs} is expressed as

$$\sigma_{abs} = Q_{abs} \pi a^2 , \qquad (18)$$

where Q_{abs} is the absorption efficiency of FUV photons by the grains. Since the UV absorption properties of PAHs and small aromatic grains are dominated by the π electron system, as for graphite, we have adopted σ_{abs} from the calculation for small graphitic grains by Draine & Lee (1984). For particles small compared to the wavelength (i.e., Rayleigh limit) σ_{abs} scales with grain volume, i.e., the number of carbon atoms. We have therefore scaled the absorption cross section of 30 Å graphite grains (Draine & Lee 1984) by the number of carbon atoms N_C in a spherical grain of radius a.

$$N_C = \frac{(4/3)\pi a^3 \rho_C}{m_C} \approx 0.5\left(\frac{a}{Å}\right)^3 , \qquad (19)$$

where ρ_C is the density of graphite and m_C is the mass of one carbon atom. Previous studies of the photoelectric heating by interstellar dust generally adopted the measured FUV extinction curve and the dust-to-gas ratio for the UV absorption properties. Since the observed extinction is well reproduced by Draine and Lee's calculations, our adopted ionization cross section is quite comparable with those in other studies. Our adopted values also compare well with the measured ionization cross section for the small PAH coronene (Fig. 1) taken from Verstraete et al. (1990).

Having considered the component terms of J_{pe}, it can be seen there are three places N_C enters into the photoelectric ejection rate. First, the absorption cross section of the grain σ_{abs} depends linearly on the number of carbon atoms. Secondly, the photoelectric yield enhancement $f_y(N_C)$ for small grains over bulk graphite depends on N_C through α and ζ. Third, the photoelectric yield and the ionization frequency depend on the ionization potential, which itself is a function of
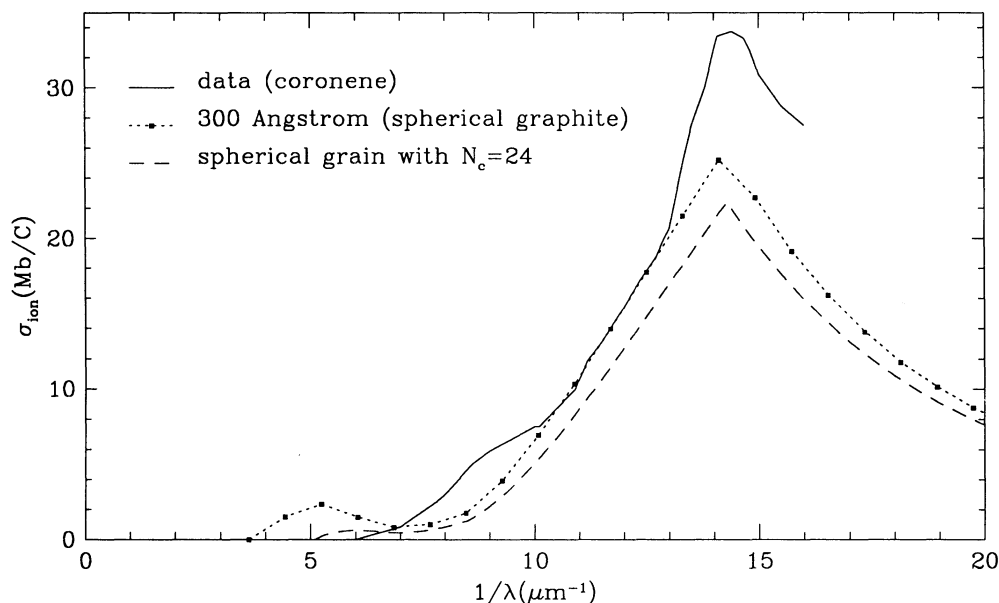

FIG. 1.—Comparison between the measured ionization cross section of coronene (taken from Verstraete et al. 1990) and that calculated using our formalism for a spherical grain composed of 24 carbon atoms. Also shown is the ionization cross section for a grain of radius 100 Å. Units are MegaBarn (10^{-18} cm^2) per carbon atom.

N_C. The dependence of σ_{abs} on N_C may be removed by considering J_{pe}/N_C, leaving only the indirect dependence through the ionization potential. It is thus possible to plot J_{pe}/N_C, leaving only the indirect dependence through the ionization potential. It is thus possible to plot J_{pe}/N_C against IP_z for both ionization energies and electron affinities and obtain a single curve to which we may fit an analytic function for J_{pe}/N_C exclusively in terms of IP_z. This value may then be scaled up by f_y. We have numerically evaluated J_{pe}/N_C (Fig. 2) and derived a single analytical fit for $T_{eff} = 3 \times 10^4$ K.

$$\frac{J_{pe}}{N_C f_y(N_C)} = 2.5 \times 10^{-13}(13.6 - IP_z)^{1.983} \text{ electrons s}^{-1}, \quad (20)$$

where the ionization potential IP_z is in eV. This expression is valid for the interstellar radiation field in the solar neighborhood. For larger fluxes, simply multiply by G_0, the ratio of the interstellar radiation field to that in the average ISM. A comparison of the numerical evaluation of J_{pe}/N_C and the analytic fit to the data points agrees to better than 60% for the whole range of ionization potentials (Fig. 2).

2.1.3. The Ionization Potential

Because we are now considering a grain size distribution extended down to the molecular regime, we must also consider how this affects the energy required by an electron to escape a small graphitic dust grain. Figure 3 shows a schematic of the variation in electronic structure with cluster size. Each sp^2 hybridized C atom in a graphitic structure will form three σ bonds with surrounding C atoms (or H atoms at the edge). These sigma bonds are arranged in a planar structure. The fourth electron will form a π bond perpendicular to this plane. These conjugated π electrons (i.e., shared among the C atoms) determine largely the electronic properties of graphitic structures. There are two π level systems; the bonding (π) and antibonding (or π^*) levels. For a neutral grain, the π levels are completely filled while the π^* levels are empty. These two level systems correspond to the conduction and valence band of graphite. As for a particle in a box, the total width of these

bands is constant but the number of levels increases with cluster size; i.e., the level separation decreases. At the same time the separation between the π and π^* system decreases with increasing size. Eventually, for an infinite graphitic plane the two bands would touch. In graphite, they actually overlap due to weak interaction between the graphite planes.

Hence, despite the similarity in structure, we cannot directly use bulk graphite properties when describing the electronic structure of small clusters of PAHs. For example, the energy level separation is about 6 eV/N_C, and, hence, only species with more than 10^4 C atoms will have a level separation in the π band less than the thermal energy at 10 K. A similar number of C atoms is required to "close" the bandgap between the π and π^* levels (see Tielens, Allamandola & Barker 1987). Thus, while graphite is a semimetal whose optical properties from the UV to the FIR are determined by electronic transitions, small PAH clusters are semiconductors, and their optical properties in the IR are dominated by the vibrational modes of the C lattice. Fortunately, here we are mainly concerned with the UV absorption properties, and the energy separation between the π and π^* system is largely independent of cluster size. Thus, although the band gap decreases, the energy difference between the peaks in the electron energy level distributions remains rather constant at $\simeq 5$ eV. As a result, the UV absorption cross section per C atom of small PAHs and 300 Å graphite grains are quite similar (§ 2.1.2).

The first ionization potential of a PAH cluster corresponds now to the energy required to bring an electron from the highest occupied level (i.e., the highest π level), corresponding to the Fermi level in solid state terms, to infinity. The electron affinity is the energy released when bringing an electron from infinity to the lowest unoccupied level (i.e., the lowest π^* level). As indicated in Figure 4, the ionization potential decreases, and the electron affinity increases with increasing PAH cluster size. Eventually it will approach the bulk value, i.e., the work function of the bulk material. To a large extent, the increased ionization potential of small PAHs reflects the electrostatic interaction between the electron and the charged grain.
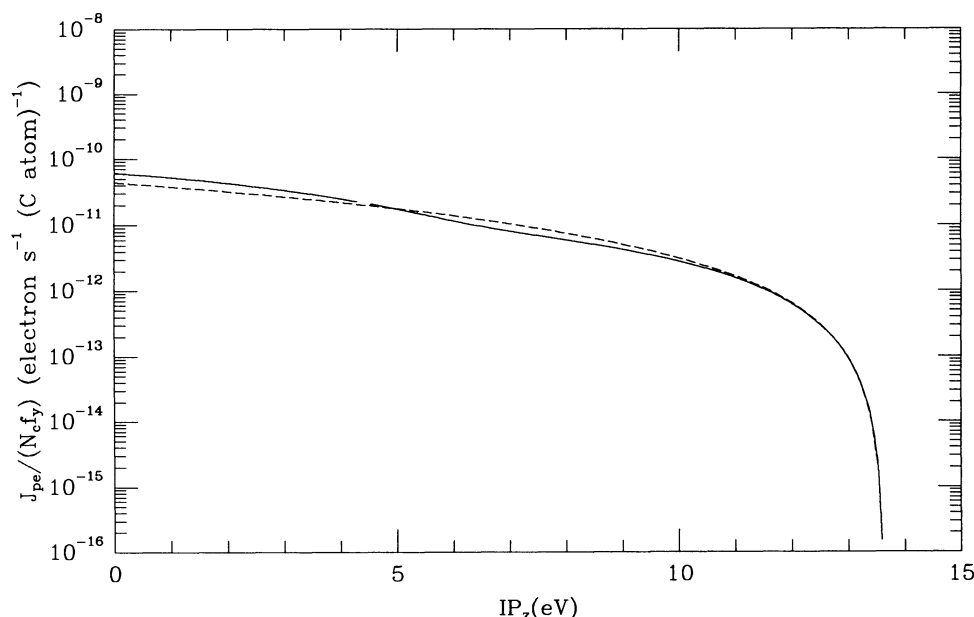

FIG. 2.—A comparison of the normalized photoelectric ejection rate, $J_{pe}/N_C f_y$, obtained via numerical computations (*solid line*) and the analytic function fitted to it (*dashed line*).
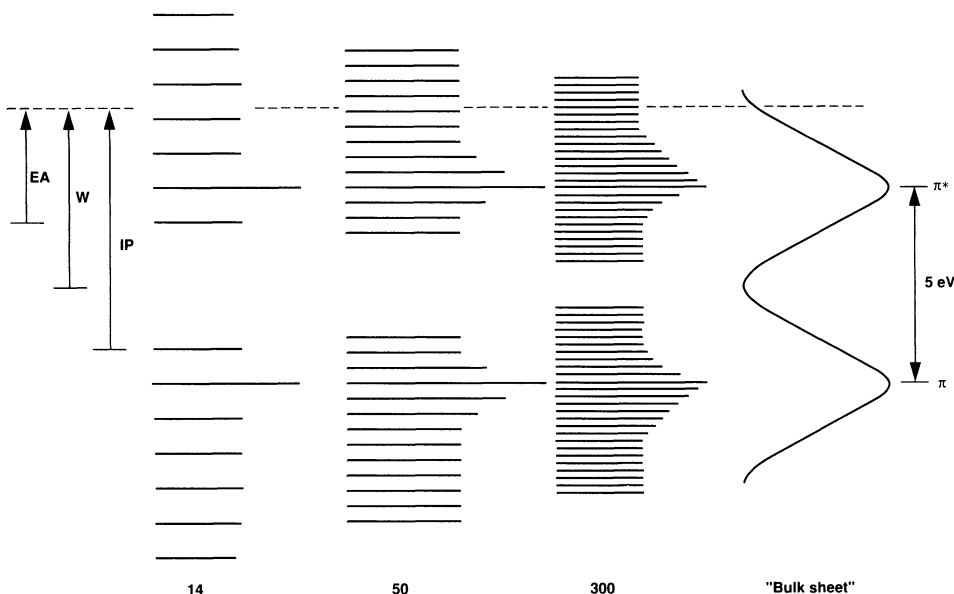
FIG. 3.—A schematic of the electronic structure of PAH clusters as a function of cluster size. See text for details.
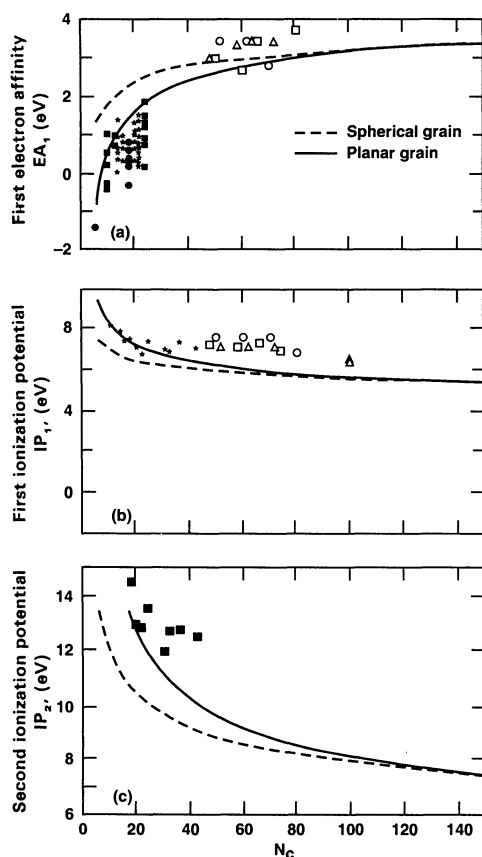

FIG. 4.—A comparison between the calculated first electron affinity and the first two ionization potentials for graphitic disks and spheres and the corresponding experimental data. Different PAH isomers are indicated by different symbols. Solid points represent planar structures, while unfilled points represent spherical shells.

Consider the process

$$A^Z \leftrightarrow A^{Z+1} + e^- ,$$
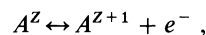
where the forward and backward arrows correspond to ionization and electron attachment, respectively. Adopting the so-called liquid drop model, the classical expression for the ionization potential (with e in esu) is

$$\mathrm{IP}_z = w + \left(Z + \frac{1}{2}\right)\frac{e^2}{C} \qquad (21)$$

(Smith 1961; Moskovitz 1991), where w is the work function of bulk graphite, and the capacitance C for a thin circular disk of radius a is given as

$$C = \frac{2a}{\pi} \qquad (22)$$

and for a spherical particle of radius a, as

$$C = a . \qquad (23)$$

Comparison of equation (21) with a large data set on small metallic clusters shows reasonable agreement. A slightly different version of this expression is sometimes used in the literature ($\mathrm{IP}_z = w + [Z + \frac{3}{8}]e^2/a$; see Wood 1981). However, this expression was derived using an unphysical model for the image charge interaction at small separation, and the older classical equation (eq. [21]) is correct. Fortuitously, the incorrect formula seemed to provide a somewhat better fit to the experimental data for small clusters than the correct one. This reflects the (small) influence of quantum effects; i.e., exchange, and correlation energies (Makov, Nitzan, & Brus 1988; Moskovitz 1991). The difference between the two expressions is, however, small. Moreover, in our case, it is dwarfed by the uncertainty in the shape and hence the capacitance of small interstellar PAH clusters (see below). Finally, we note that, strictly speaking, this equation applies to metallic species. For

a material with finite dielectric constant ϵ, the second term in equation (21) has to be multiplied by $(\epsilon - 1)/\epsilon$ (Brus 1983). However, for typical materials and particularly PAH species, this correction factor is small (see the discussion in Draine & Sutin 1987).

A value of 4.4 eV was adopted for the work function, appropriate to an infinite graphitic sheet (Smith 1961; Gallegos 1968). In terms of N_C, equation (21) for disks is given by

$$IP_z = 4.4 + \left(Z + \frac{1}{2}\right)\frac{25.1}{N_C^{1/2}}\ eV\ , \qquad (24)$$

and for spheres,

$$IP_z = 4.4 + \left(Z + \frac{1}{2}\right)\frac{11.1}{N_C^{1/3}}\ eV\ . \qquad (25)$$

These two expressions for the first ($Z = 0$) and second ($Z = 1$) ionization potential and the first electron affinity ($Z = -1$) are compared to measured data (Leach 1987; Tobita et al. 1992) for small PAH molecules (Fig. 4). The ionization potential is dependent on the grain geometry through the capacitance term and has been calculated for the circular disk geometry appropriate for compact condensed PAHs and a spherical geometry probably more appropriate for grains larger than ~ 1000 C atoms. Clearly, shape has a major effect on the ionization potential for small species. However, both disks and spheres approach the bulk work function rapidly, and for $N_C \geq 100$ C atoms the difference is very small. Since spheres probably describe the surface-volume relation for large species better than disks, we have adopted the sphere geometry throughout, including for the calculation of the ionization potential. The influence of that assumption will be assessed in § 3.3.3.

In contrast to previous theoretical studies of grain charging in the ISM (Draine 1978), we recognize that interstellar grains cannot be charged indefinitely. In particular, a grain can only acquire a certain number of negative charges before the electron affinity becomes negative and any electrons colliding with the grain spontaneously detach (see Fig. 4). Indeed, the first electron affinity for benzene ($N_C = 6$) is negative and the benzene ion autoionizes in $< 10^{-12}$ seconds (Christophorou, McCorkle, & Christodoulides 1984).

The maximum positive, Z_{IP}, and negative charges, Z_{EA}, a grain of a given radius can acquire when illuminated by photons of maximum energy equal to 13.6 eV are given by

$$Z_{EA} = \frac{wC}{e^2} - \frac{1}{2} = 0.4N_C^{1/3} - \frac{1}{2}\ , \qquad (26)$$

$$Z_{IP} = (13.6 - w)\frac{C}{e^2} + \frac{1}{2} = 0.87N_C^{1/3} + \frac{1}{2}\ , \qquad (27)$$

where the right-hand side pertains to spheres. This maximum number of negative charges is considerably less than that required for field emission of bulk graphite (Draine 1978). Essentially, while for bulk graphite the electron affinity remains tied to the energy of the Fermi level, the electron affinity decreases with radius for small clusters (Fig. 4).

2.2. The Photoelectric Heating Rate

The photoelectric heating rate $H(N_C)$ for a grain with N_C carbon atoms and charge Z is given by

$$H(N_C) = W\pi \int_{\nu_Z}^{\nu_H} \sigma_{abs}\ Y_{ion}\ B_\nu\ g(N_C, IP_z)d\nu\ . \qquad (28)$$

The kinetic energy partition function $g(N_C, IP_z)$, defined as the fraction of the photon energy carried away by a photoejected electron, is assumed to be given by

$$g(N_C, IP_z) = \frac{1}{2}\left(\frac{h\nu - IP_z}{h\nu}\right)\ . \qquad (29)$$

The form of this function is such that at high photon energies, half of the photon energy is carried away by the photoejected electron, while the remainder is dissipated in the excitation energy of the species. There is some experimental support for this from studies of the benzene, coronene, and ovalene molecules (see Léger & d'Hendecourt 1987) and bulk graphite (see Feuerbacher, Willis, & Fitton 1973). This quantity is, however, still quite uncertain.

The terms σ_{abs}, Y_{ion}, IP_z, and $g(N_C, IP_z)$ of this frequency-dependent integral are all dependent on the size of the dust grain considered. As for the photoelectric ejection rate, the direct dependence on N_C can be factored out (see eq. [20]), and an analytic function dependent only on IP_z can be fitted to the numerical results to represent the heating rate per C atom.

$$\frac{H(N_C)}{f_y N_C} = 1.4 \times 10^{-25}\left(13.6 - \frac{IP_z}{eV}\right)^{2.987}\ ergs\ s^{-1}\ . \qquad (30)$$

This analytical expression is compared to the detailed numerical calculations in Figure 5. It is dependent on the effective temperature of the illuminating source, and in this case $T_{eff} = 3 \times 10^4$ K.

2.3. The Grain-Ion Recombination Cooling Rate

Charged particles adhering to a grain surface remove energy from the surrounding gas at a rate per grain (Draine & Sutin 1987) given by

$$C(N_C, Z) = n_i s_i\left(\frac{8kT}{\pi m_i}\right)^{1/2}\pi a^2 \tilde{\Lambda}\left(\tau = \frac{akT}{q_i^2},\ \nu = \frac{Ze}{q_i}\right)kT\ . \qquad (31)$$

As with the grain charging analysis, there are three cases. For a neutral grain where $\nu = 0$, the exact result is

$$\tilde{\Lambda}(\tau,\ \nu = 0) = 2 + \frac{3}{2}\left(\frac{\pi}{2\tau}\right)^{1/2}\ . \qquad (32)$$

For an attractive Coulomb potential where ν is negative,

$$\tilde{\Lambda}(\nu < 0) \approx \left(2 - \frac{\nu}{\tau}\right)[1 + (\tau - \nu)^{-1/2}]\ , \qquad (33)$$

accurate to $\pm 10\%$ for $\tau > 0.1$. For a repulsive Coulomb potential where ν is positive, then,

$$\tilde{\Lambda}(\nu > 0) \approx \left(2 + \frac{\nu}{\tau}\right)\left[1 + \left(\frac{3}{2\tau} + 3\nu\right)^{-1/2}\right]\exp\left(\frac{-\theta_\nu}{\tau}\right)\ , \qquad (34)$$

accurate to within $\pm 5\%$ for $\tau > 10^{-3}$.

2.4. The Grain Size Distribution

Because we have formulated our analysis in terms of the number of carbon atoms N_C in a grain of a certain radius and geometry, the grain size distribution must be written in terms of N_C also. Studies of the IR emission of the galaxy have shown that the interstellar grain distribution as derived from optical and UV extinction measurements [i.e., $n(a) \sim a^{-3.5}$; see Mathis, Rumpl, & Nordsieck 1977; Draine & Lee 1984] extends well into the molecular domain (Tielens 1990). Hence,
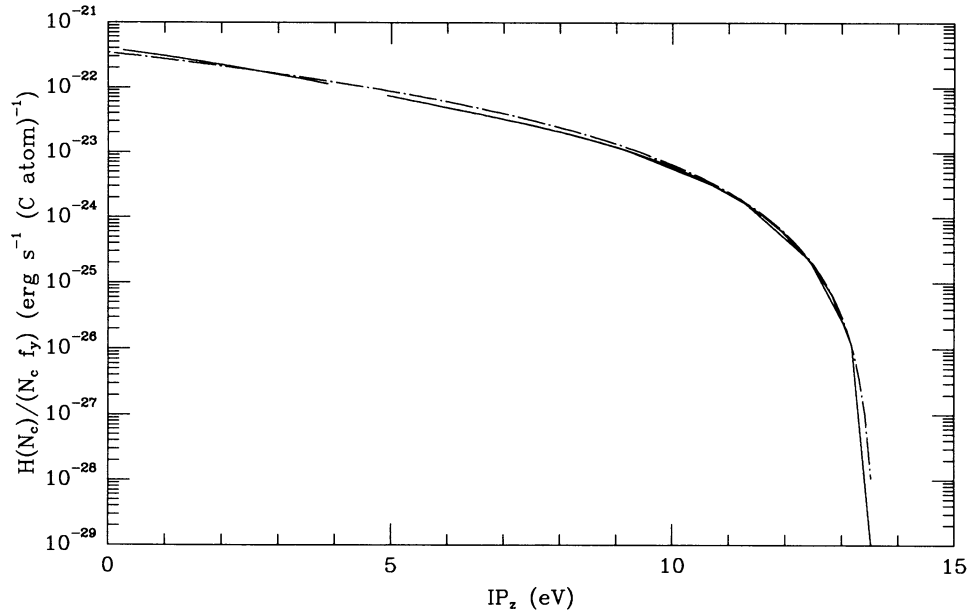
FIG. 5.—The normalized heating rate, $H/N_c \, f_y$, as a function of ionization potential, IP_z. Solid line is the numerical results. Dashed line is the analytical fit.

we can write

$$n(N_C)dN_C = B_C \, N_C^{-\beta} \, dN_C \, , \qquad (35)$$

where $\beta = 11/6$ and B_C is 1.24×10^{-6} grains (C atom)$^{5/6}$ (H atom)$^{-1}$. The number of carbon atoms in a grain with size a is given by equation (19).

3. RESULTS

The effective heating rates are calculated from equation (3), where H (N_C) is given by equation (1) as a function of the ionization potential, and the number of carbon atoms in the grain and the enhancement factor $f_y(N_C)$ follows from equation (16). The ionization potential as a function of grain size is given by equation (21). The ionization fractions $f(N_C, Z)$ follow from solving the ionization balance (eqs. [6]–[7]) with the photoelectric ionization rate given by equation (20) and the recombination rates given by equation (9). The cooling rates $C(N_C, Z)$ are given by equation (31). Finally, the grain size distribution is given by equation (35).

3.1. Free Parameters

The free parameters in our model are B_C, β, N_- and N_+, which describe the grain size distribution, the electron escape length, l_e, the photon attenuation length, l_a, the effective temperature T_{eff}, and the total intensity of the incident radiation field G_0. Standard values for these parameters are given in Table 1, although the variation of T_{eff} is left for future publications.

The grain charge distribution is largely a function of G_0, n_e, and T. We have investigated a wide variety of physical conditions in the interstellar medium, summarized in Table 2, where n_H is the hydrogen nucleus density, and the fractional ionization of the gas X_e is given by the ratio of the electron density to the hydrogen nucleus density. As expected, the grain charge distribution depends on the ratio G_0/n_e.

Although the $T_{eff} = 3 \times 10^4$ K blackbody radiation field is not entirely appropriate to the cold diffuse ISM, it is still ade-

quate to use when comparing results for the three different types of ISM. The variation of l_e and the maximum and minimum bounds of the range for the MRN distribution and the value of β are investigated to determine their effects on the grain charge distribution.

3.2. The Grain Charge Distribution

Figure 6 shows the grain charge distribution function $f(N_C, Z)$ for three grain sizes in the standard Tielens & Hollenbach

TABLE 1
MODEL PARAMETERS AND VALUES

Parameter	Value
MRN grain size distribution in terms of radius	$A_i a^{-\alpha} n_H \, da$
Lower limit on grain radius (cm)	3.1×10^{-8}
Upper limit on grain radius (cm)	1.0×10^{-6}
α	3.5
A_i	$10^{-25.16}$
MRN grain size distribution in terms of N_C	$B_C \, N_C^{-\beta} n_H \, dN_C$
N_-, lower limit on N_C	14
N_+, upper limit on N_C	4.6×10^5
β	11/6
B_C	1.24×10^{-6}
Electron escape length l_e (cm)	10^{-7}
Photon attenuation length l_a (cm)	10^{-6}
Effective temperature T_{eff} (K)	3×10^4

NOTES.—The standard values for the free parameters in the grain size distribution, the electron escape length, the photon attenuation length and the effective temperature of the illuminating source are shown.

TABLE 2
STANDARD PARAMETERS FOR INVESTIGATION OF THREE TYPES OF ISM

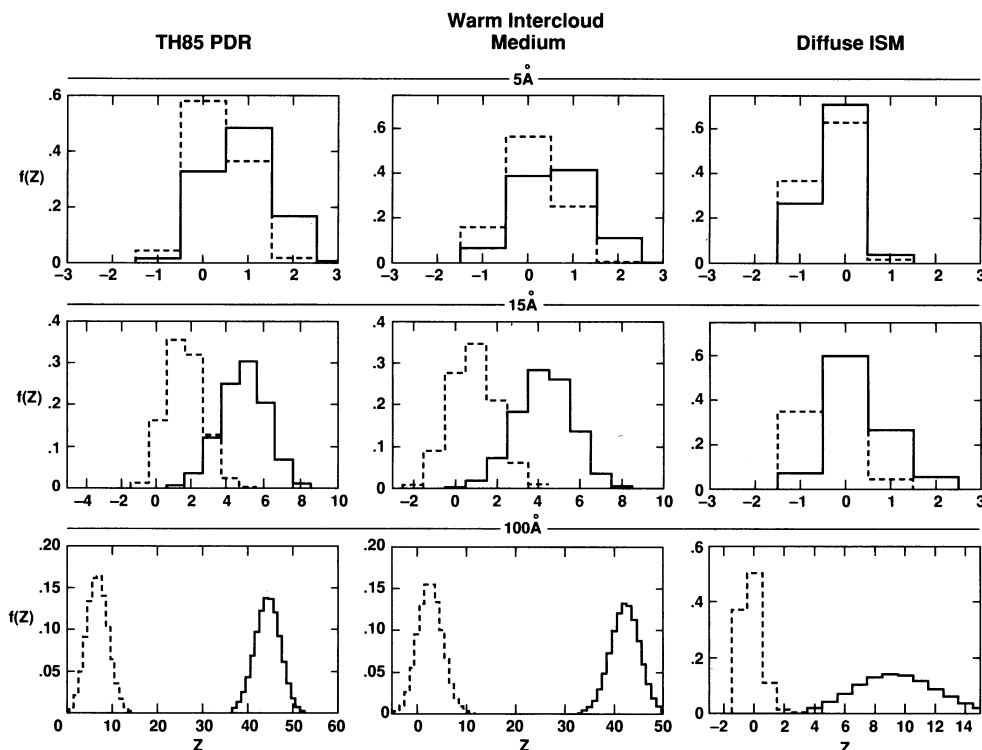| Interstellar Region	$n_H(cm^{-3})$	G_0	T (K)	X_e
TH85 PDR model	2.5×10^5	10^5	10^3	3×10^{-4}
Warm intercloud medium	0.25	1	8×10^3	1×10^{-2}
Cold diffuse cloud	25.0	1	100	3×10^{-4}

FIG. 6.—A comparison of the charge probability function for spherical grains of radius 5, 15, and 100 Å in the TH85 PDR PDR model, the WIM and the DIM. Solid line represents a spherical particle, and the dotted line is a planar particle of the same radius.

(1985) PDR model (hereafter TH85), the warm neutral ISM, and the cold diffuse ISM. The corresponding average grain charge $\langle Z \rangle$ is shown in Figure 7. Ignoring the temperature dependence for the moment, the grain charge distribution depends on the ratio of the ionization rate over the recombination rate, which in turn depends on G_0/n_e. Consider, for simplicity, a species which has only two ionization stages, 0 and 1. The neutral fraction is given by

$$ f(0) = (1 + \gamma)^{-1} , \tag{36} $$

with γ being the ionization rate over the recombination rate given by

$$ \gamma = \gamma_0 \, f_y(N_C) N_C^{2/3} \frac{G_0 \, T^{1/2}}{n_e} , \tag{37} $$

where γ_0 is equal to 3×10^{-6}. Thus, when G_0/n_e increases, the neutral fraction $f(0)$ decreases. This trend of decreasing $f(0)$ with increasing G_0/n_e is confirmed by detailed calculations (see $a = 5$ Å in Fig. 6). For small PAHs ($a < 15$ Å), two relevant ionization stages is a reasonable approximation. For diffuse clouds we then find $\gamma < 1$ and, hence, most species are neutral. For the warm intercloud medium, however, γ becomes larger than 1, and the grains will charge up.

As grain size increases up to 100 Å, the photoelectric ionization rate increases with the number of carbon atoms in the grain, while the recombination rate generally increases much more slowly (as $N_C^{1/3}$ for $\tau \ll 1$ and $N_C^{2/3}$ for $\tau \gg 1$; see § 2.1.3.). As a result, grain charge increases with increasing grain size and the charge distribution shifts toward higher positive charge (see eq. [36] and eq. [37]). These considerations are borne out by our numerical results (see Fig. 6). The electron escape length l_e (i.e., the probability that the electron created in

a species reaches the grain surface) has only a relatively small effect. It increases the ionization rate by an order of magnitude from bulk graphite to coronene ($N_C = 24$ C atoms). However, the ratio of the ionization rate to the recombination rate scales with $N_C^{2/3}$, and this ratio increases by a factor 8/3. This means that the neutral fraction decreases by almost two orders of magnitude over the grain radius range and dominates over the yield enhancement. For larger species, the same dependence on G_0/n_e, where grain charge increases with radius, is still evident, although more ionization stages are involved. The temperature dependence which enters through the recombination rate is somewhat complicated. For neutral species, the recombination rate has no temperature dependence for large effective temperatures (i.e., large τ), while positively charged species show a $T^{-1/2}$ dependence due to Coulomb focusing (see eqs. [9] and [11]).

The results discussed above pertain to spherical grains. For the same number of C atoms, disks have a larger geometric cross section and hence a larger recombination rate than spheres. The ionization potential of disks is lower, while the electron affinity is higher than for spheres (see eqs. [24] and [25]). Thus, the ionization rate for neutral disks is slightly higher, while for negatively charged disks it is slightly lower than for spheres. Overall, the first effect is dominant, however, and disks have somewhat lower charge than corresponding spheres (see Fig. 6). In particular, we conclude that PAHs with $N_C \lesssim 100$ carbon atoms are predominantly in the form of anions or neutrals in diffuse interstellar clouds. In contrast to previous studies (Crawford, Tielens, & Allamandola 1985; Léger & Puget 1984), cations have a very low abundance. Essentially, those studies were based upon an electron-PAH cation recombination rate which was too low. We note therefore that, if small PAHs are the carriers of the diffuse inter-
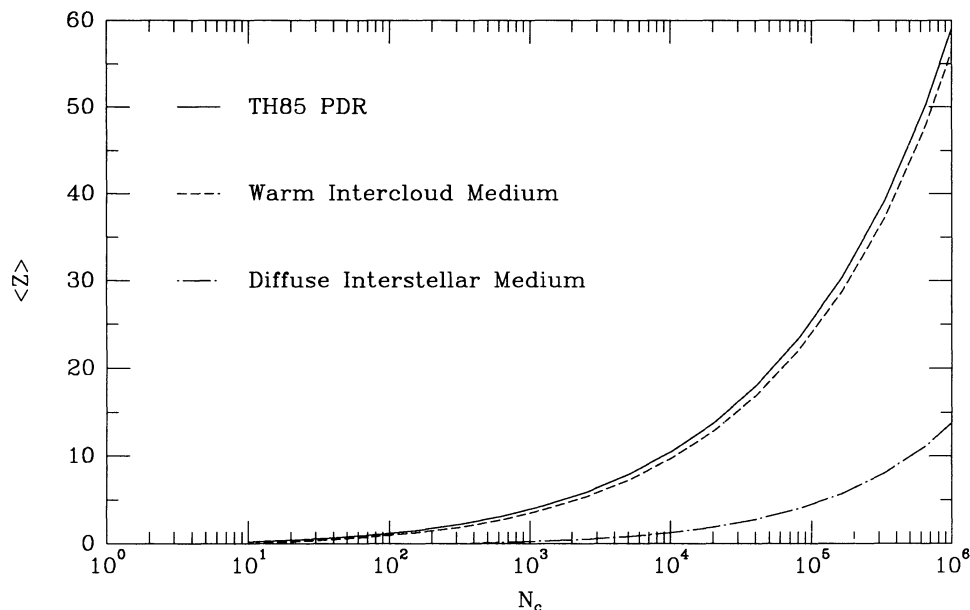
Fig. 7.—A comparison of the average charge for spherical grains composed of N_C carbon atoms in the TH85 PDR model, the WIM, and the DIM

stellar bands, their visual absorption is possibly due to their anionic state, not their cationic state.

3.3. The Photoelectric Heating Rate

The net photoelectric heating rate, Ψ, by species with N_C C atoms is shown in Figure 8 for the TH85 PDR model conditions. Other conditions show the same trend of decreasing heating with increasing grain size. Quantitatively, this means that for gas temperatures up to 10^4 K, there is a change of less than 25% in the gradient of the total heating rate ΨN_C over five orders of magnitude of $G_0 T^{0.5}/n_e$. The photoelectric heating rate increases rapidly with decreasing grain size, and "classical" grains ($a \sim 1000$ Å) contribute negligibly to the total heating rate (see Watson 1972). Indeed, approximately

half of the total heating is due to species with $N_C \leq 1500$ carbon atoms ($a \leq 15$ Å). The other half is contributed by the larger species up to 4.6×10^5 carbon atoms ($a \leq 100$ Å) (Fig. 8). Modeling the photoelectric heating effect using a "typical" PAH as the only intermediary between incoming photons and the surrounding gas is incomplete. It is important that a grain size distribution is considered in a study of photoelectric heating; otherwise, half of the total gas heating is lost.

For species which are small compared to the wavelength ($a \leq 300$ Å; $N_C \leq 10^7$), the UV absorption cross section scales with N_C, and, hence, the fraction of UV energy absorbed by all grains of size N_C scales with $N_C^{1/6}$. Thus, the efficiency of the photoelectric heating, that is, the efficiency with which absorbed UV photons are transformed into gas heating,
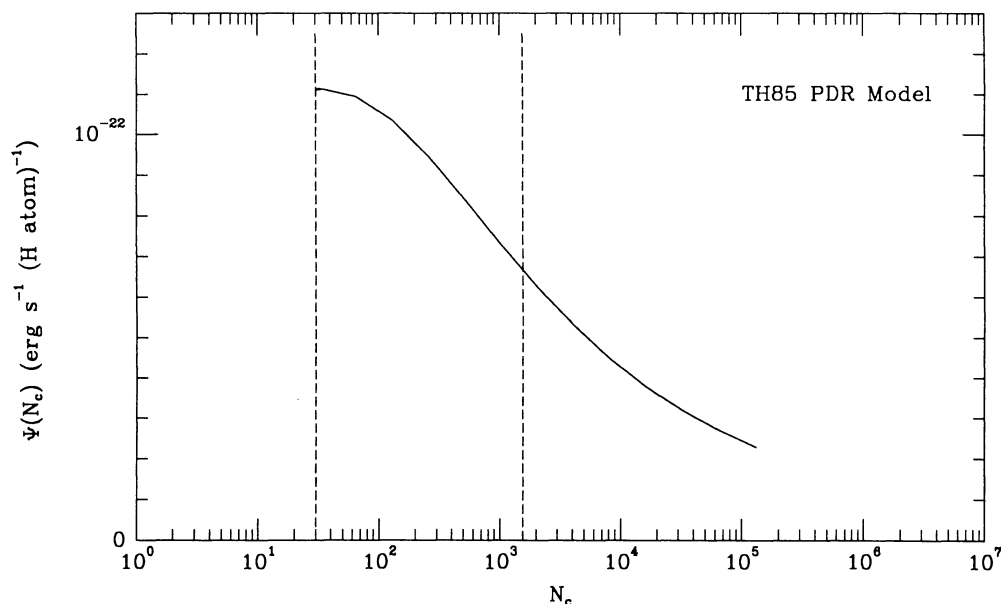

Fig. 8.—Contribution to the photoelectric heating rate, Ψ, as a function of grain size

decreases even more rapidly with increasing grain size than Ψ itself. This decrease in the photoelectric efficiency with increasing grain size results partly from the decrease in yield (i.e., f_y), which decreases by an order of magnitude from the small to the large grains in our size distribution. It is further aided by the increase in the average grain charge with increasing grain size, which is a direct result of the fact that the UV absorption rate (i.e., the ionization rate) increases proportionately to N_C (or, the grain volume), while the recombination rate depends only weakly on N_C (see eq. [37]). The contribution of the smallest PAHs to the photoelectric heating rate levels off because they reach their maximum negative charge, and further reduction of the ionization rate over the recombination rate with decreasing grain size cannot lead to smaller Z (Fig. 8).

3.3.1. The Variation of the Photoelectric Heating Rate with l_e

We have investigated the effects of varying the electron escape length on the total heating rate. In our formalism, an increase in l_e leads to a smaller enhancement of the photoelectric yield over bulk graphite so that f_y decreases. Hence, since our photoelectric yield is normalized to that measured for bulk graphite, the yield for small PAHs decreases with increasing l_e. As a result, they become even less positively charged, and their contribution to the photoelectric heating rate increases. In contrast, this plays less of a role for larger species (Fig. 9).

If we had chosen to normalize our photoelectric yield to that measured for small PAHs rather than to bulk graphite, an increase in l_e would have led to an increased yield for larger grains (and none for PAHs). In that case, the charge of the larger grains would become more positive, and this would result in a decrease in the contribution of the large grains relative to that of PAHs. Note that with this latter normalization, the total photoelectric heating rate decreases with increasing l_e.

As emphasized in § 2, experiments on bulk graphite support the adopted value of l_e in our standard model. Moreover, within our formalism, this value reproduces both the measured low yield for graphite and the high yield for small PAHs. As a consequence, we recommend using the standard value for l_e.

Finally, as originally envisioned by Watson (1972), the enhancement of the yield for small grains over bulk graphite implies that the former dominates the photoelectric heating of the interstellar gas. As our numerical results illustrate, l_e has an important effect on the heating rate. It is further enhanced by the lower average charge of small grains relative to large ones (see § 3.2).

3.3.2. Variation in the Grain Size Distribution

We varied the grain radius index, α, in the Mathis, Rumpl, and Nordsieck (hereafter MRN) grain size distribution from -3.5 to -4.0 and -4.5 while keeping the total number of carbon atoms in the grain population with $N_C < 10^6$ constant. The more negative the index, the more enhanced the number density of the small grain population relative to the large. Figure 10 illustrates the variation in the heating rate as a function of the grain size for the standard TH85 PDR model. As expected, when the abundance of small species increases relative to the large ones, their contribution to the heating increases as well. Because of the normalization of the grain size distribution, a more negative α results in fewer larger grains, and, hence, their contribution decreases. Comparing the total heating rates Γ_{pe}, we conclude that varying α from -3.5 to -4.0 to -4.5 leads to an increase in Γ_{pe} of a factor 2 and 3, respectively.

The lower limit of the grain size distribution has a considerable influence on the total photoelectric heating rate. Increasing the lower limit from 14 to 1555 C atoms (3 Å to 15 Å) halves the total heating rate. Increasing the lower limit even further to 100 Å reduces the heating by a factor of ~ 10. The upper limit of the grain size distribution, on the other hand, has little influence on the total heating rate (see Fig. 10). Increasing the upper size limit to 300 Å (3×10^7 C atoms) increases the total heating rate by only 10% for typical diffuse cloud conditions (i.e., low grain charge) and even less for more highly charged environments.

3.3.3. Disks Versus Spheres

While large grains (≥ 1000 C atoms) are likely to be spheres, small species (≤ 100 C atoms) will resemble PAH molecules,
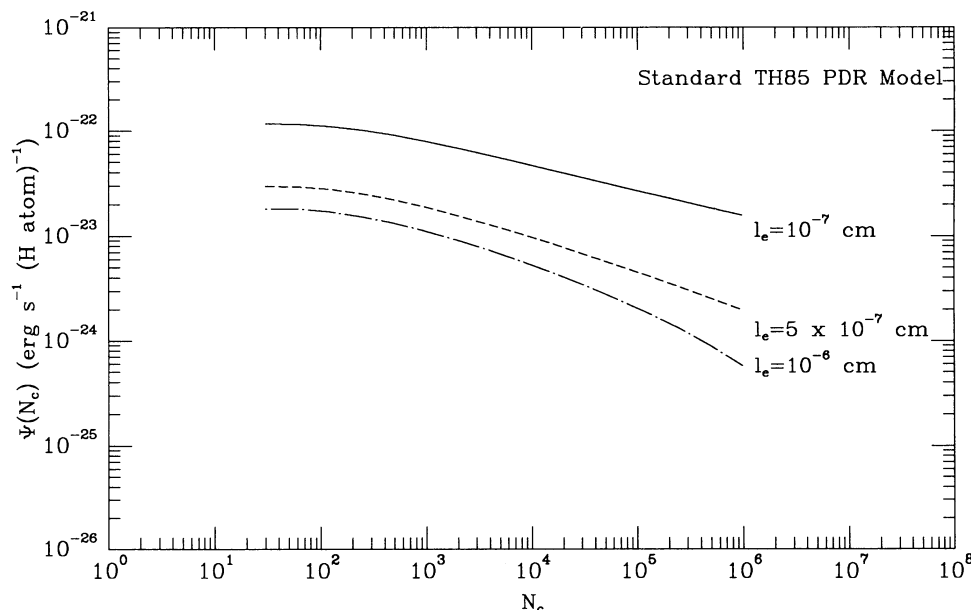

FIG. 9.—The effects of varying electron escape length, l_e, on the heating rate in the TH85 PDR model parameter environment
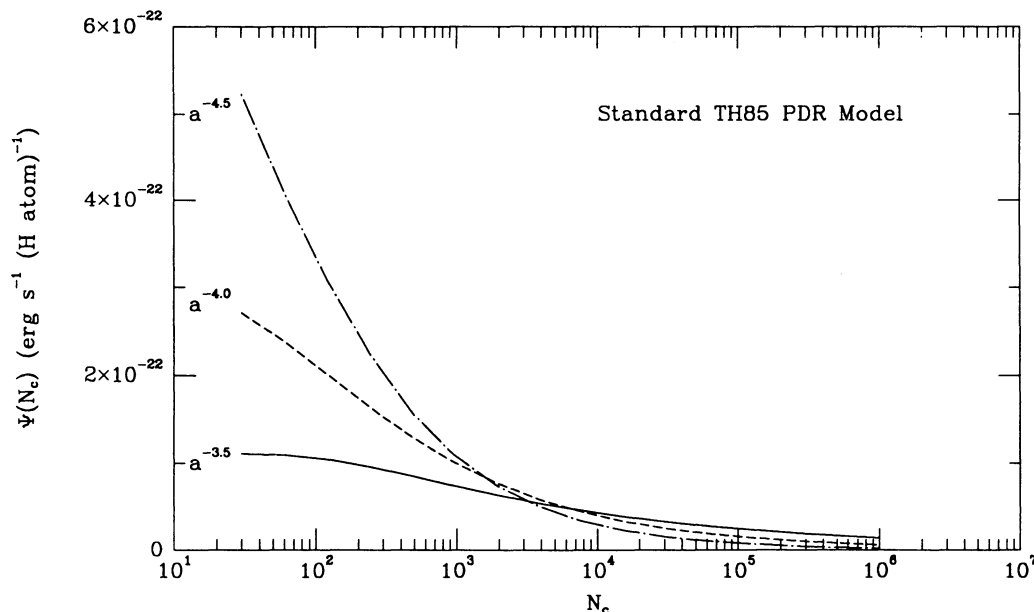
FIG. 10.—The effects of varying the slope of the grain size distribution on the heating rate in the TH85 PDR model parameter environment. The total number of carbon atoms in the grain population is kept constant.

which are planar. In between, the species are likely to consist of stacks of smaller species bonded by weak van der Waals forces or by peripheral aliphatic groups (Tielens 1990). In our analysis, we have adopted for simplicity a spherical shape for all sizes. Shape has a subtle effect on the heating. First, it will influence the ionization potential (see eqs. [24] and [25]). Neutral or positively charged disks, therefore, have a higher $J_{pe}/N_C f_y$ than spheres for the same number of carbon atoms, reflecting their lower ionization potential. Disk anions, on the other hand, will have a lower $J_{pe}/N_C f_y$ due to their higher electron affinity (Fig. 4). Furthermore, because of their large surface area, electrons can escape more easily from disks than from spherical grains, and, hence, f_y is larger. Most importantly, however, for the same number of carbon atoms, a disk is larger than a sphere, and thus the recombination rate is higher. As a result, disks are less positively charged than spheres with the same number of carbon atoms (Fig. 6), and, hence, the efficiency of the photoelectric heating increases. However, any difference in thermal behavior between neutral disks and spheres is small.

4. THE PHOTOELECTRIC HEATING EFFICIENCY

We have numerically investigated the grain charge distribution functions and the photoelectric heating rate for a wide range of physical conditions ($1 < G_0 < 10^5$; $2.5 \times 10^{-3} < n_e < 75$; $10 < T < 10,000$ K). The photoelectric heating rates have been converted into heating efficiencies by ratioing to the total UV photon energy absorbed by all grains. The latter is given by $\simeq 8.1 \times 10^{-26}(N_+^{1/6} - N_-^{1/6})$ ergs s^{-1} (H atom)$^{-1}$ with N_+ and N_- the limits in the size distribution considered. For our purposes, FUV extinction is dominated by small grains ($a < 300$ Å), and the total absorbed energy is about 10^{-24} ergs s^{-1} (H atom)$^{-1}$. Note, however, that half of the UV photon energy is absorbed by grains larger than 100 Å, which do not contribute to the gas heating at all.

The results for the efficiency are shown in Figure 11 as a function of $G_0 T^{1/2}/n_e$. For $T < 4000$ K, the efficiency forms a

simple relationship which reflects directly the variation in the grain charge. We can estimate the heating efficiency from equation (30) to be approximately equal to

$$\epsilon = 7.3 \times 10^{-6}\left(13.6 - \frac{\overline{IP}_z}{eV}\right)^3 \langle f_y \rangle \langle f(0) \rangle . \qquad (38)$$

Our numerical results show that approximately half the heating originates from $a < 15$ Å. With a typical ionization potential of 5.5 eV and a yield enhancement factor of 8, we find

$$\epsilon = 3 \times 10^{-2} \langle f(0) \rangle . \qquad (39)$$

For neutral grains, the limiting heating efficiency is thus 0.03. About half of the photons are absorbed by grains < 100 Å and can thus lead to gas heating. With an average ionization potential of 5.5 eV, the typical ionization yield for small neutral PAHs is about 0.4 (see eq. [15]), and about a fraction of 0.15 is available for heating (see eq. [29]). Hence, this limits the efficiency to 0.03 for neutral grains.

The typical neutral fraction, $\langle f(0) \rangle$, can be evaluated from equation (36). Hence,

$$\epsilon = \frac{3 \times 10^{-2}}{1 + 4.2 \times 10^{-4} G_0 T^{1/2}/n_e} . \qquad (40)$$

The neutral fraction depends on the ratio of the ionization and recombination rates, which itself depends on $G_0 T^{1/2}/n_e$. An increase in G_0 leads to an increase in the ionization rate; hence, the neutral fraction will decrease, and the heating efficiency will decrease. Conversely, an increase in the electron abundance leads to a larger neutral fraction and thus a higher heating efficiency. Because of Coulomb focusing, an increase in T actually leads to a decrease in the recombination rate, a smaller neutral fraction, and therefore lower heating efficiency.

Essentially all grains will attain many different photoionization stages under typical conditions (see Fig. 6). Hence, singly and more highly charged grains can also contribute to the photoelectric heating, albeit at a reduced efficiency due to their higher ionization potential (see Fig. 5). For a single size of
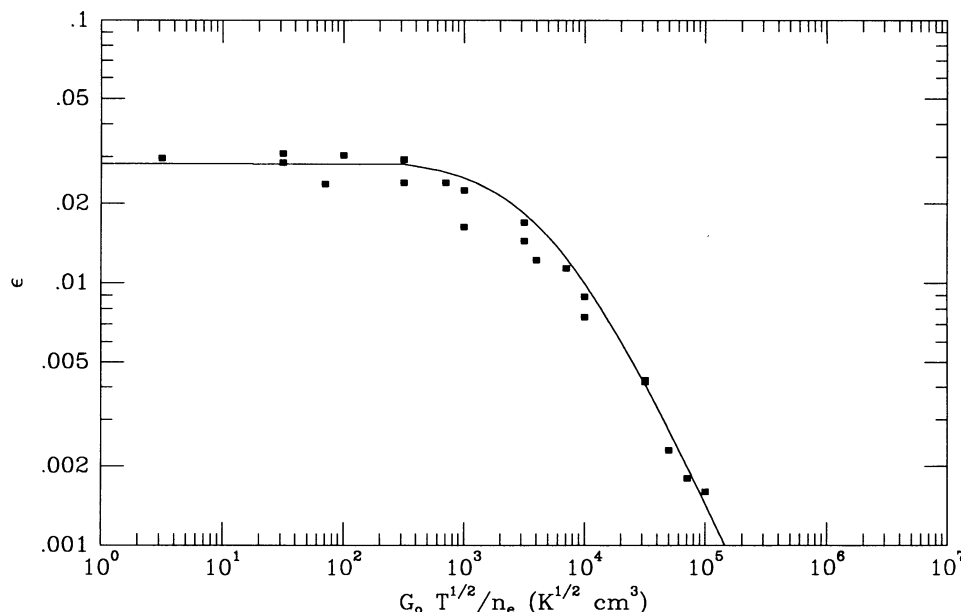
FIG. 11.—The numerically calculated efficiency (*squares*) of the net photoelectric heating rate per hydrogen atom for a range of different interstellar environments defined by the intensity of the incident UV field, G_0, gas temperature, T, and electron density, n_e. The analytic fit (*solid line*) compares well with the numerical results for all gas temperatures less than 10^4 K.

grain, this can be incorporated into a semianalytical formalism (see de Jong 1977), but a grain size distribution complicates such an approach even further. Nevertheless, the essential characteristic, decreasing heating efficiency with increasing grain charge, is still preserved. Indeed, the numerical results for $T < 10,000$ K show a good correlation with $G_0 T^{1/2}/n_e$. For higher temperatures ($kT \sim 1$ eV), recombining electrons can lead to appreciable cooling of the gas. The simple considerations discussed above can then lead to too high a net heating rate.

Following this discussion, an analytical expression is fitted to the photoelectric heating efficiency as a function of $G_0 T^{1/2}/n_e$:

$$\epsilon = \frac{3 \times 10^{-2}}{1 + 2 \times 10^{-4} G_0 T^{1/2}/n_e} . \tag{41}$$

Figure 11 shows the match between the numerical evaluation of photoelectric heating efficiency compared with the analytic fit above. The comparison is very favorable for gas temperatures up to 10^3 K. The coefficient in the denominator is slightly different from that derived by the simple model above, likely reflecting the presence of size and charge distributions.

5. THE HEATING OF THE ISM

5.1. *The Heating of the Diffuse ISM*

In this section we will use the heating formalism developed in the preceding sections to realistically model the heating of the interstellar medium. To that end, we have made two changes. First, we have adopted the shape of the interstellar radiation field as derived by Draine (1978). However, for consistency, we have normalized the total integrated intensity of the field to that derived by Habing (1968) (1.6×10^{-3} ergs cm^{-2} s^{-1}). Essentially, this adds a large visible photon flux. Second, the small size limit of the interstellar grain size distribution is likely to be dominated by PAH molecules. Hence, these are likely to be disk shaped rather than spheres. For

simplicity, we have assumed that all particles smaller than 15 Å radius are circular disks, while the larger ones are spheres. We have adopted the MRN grain size distribution for both regimes [i.e., $n(a)$ scales with $a^{-3.5}$]. For comparison and consistency with our previous results, we have normalized the total volume in disks (i.e., total number of carbon atoms) to that in the MRN size distribution between 3 Å and 15 Å. In terms of the number of carbon atoms per species N_C, the distribution is then given by $n(N_C)dN_C = 1.15 \times 10^{-5} N_C^{-2.25} dN_C$ between 12 and 275 carbon atoms. There are ≈ 2.5 times more disks in this distribution than there are spheres with $a < 15$ Å in the MRN distribution.

Figure 12 shows the calculated heating rate as a function of the grain charge parameter $G_0 T^{0.5}/n_e$ for three different gas temperatures. The overall heating rate is slightly higher
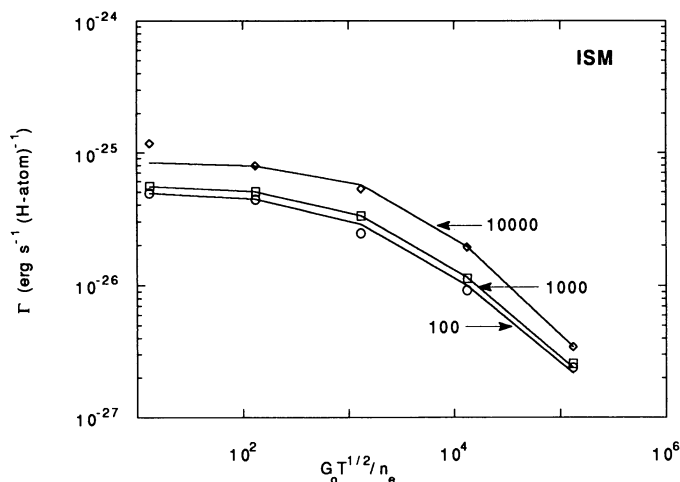

FIG. 12.—Calculated heating rate as a function of the grain charge parameter $G_0 T^{0.5}/n_e$ for three different gas temperatures for a mixed disk and sphere population, discussed above.

($\approx 50\%$) than that given by equation (41) for pure spheres. About half of this difference is due to the different shape of the interstellar radiation field and about half to the different grain geometry. The results are fairly robust to these uncertain parameters. While there are many more disks than spheres, this has little influence on the resulting heating rate. For a neutral grain (i.e., small grain charge parameter), the heating efficiency per absorbed UV photon is similar for a disk and a sphere. Since the disk/sphere distribution has the same total number of C atoms as the pure sphere case, the total number of UV photons absorbed and, thus, the total heating rate, is also very similar. For increasing $G_0 T^{0.5}/n_e$, the grains charge up and the photoelectric heating efficiency decreases. At this stage, the heating rate becomes proportional to the grain-electron recombination rate. Comparing a disk and a sphere of the same radius, the sphere will be more highly charged for the same $G_0 T^{0.5}/n_e$. This means the grain-electron recombination rate (and hence the heating rate) is higher due to Coulomb focusing. However, there are more disks than spheres in the grain distribution, and this more than compensates for the difference in recombination rate per grain.

We note that the heating rate increases with gas temperature as it approaches 10^4 K. This reflects an increase in the grain-electron recombination rate with increasing temperature at those high gas temperatures. The Coulomb focusing effect ($\tau \sim 1$; Draine & Sutin 1987) becomes negligible. At higher temperatures, the grains become more highly negatively charged with increasing gas temperature. This results in a decrease in the grain ionization potential and an increase in the photoelectric heating rate.

The total heating rate for very small graphitic grains and PAHs is given by

$$\Gamma_{\rm pe} = 10^{-24}\epsilon G_0 n_{\rm H} \quad {\rm ergs\ s^{-1}\ cm^{-3}}, \qquad (42)$$

where for gas temperatures up to 10^4 K, ϵ is given by

$$\epsilon = \frac{4.87 \times 10^{-2}}{[1 + 4 \times 10^{-3}(G_0 T^{1/2}/n_e)^{0.73}]}$$
$$+ \frac{3.65 \times 10^{-2}(T/10^4)^{0.7}}{[1 + 2 \times 10^{-4}(G_0 T^{1/2}/n_e)]}. \qquad (43)$$

For low $G_0 T^{1/2}/n_e$ and hence neutral grains, the total heating rate is about $5 \times 10^{-26}G_0$ ergs s^{-1} (H atom)$^{-1}$ and scales linearly with the intensity of the incident UV field. For high $G_0 T^{1/2}/n_e$, the total heating rate is independent of the intensity of the incident UV field and scales with the product $n_e n_{\rm H}$. At this point, most grains are positively charged, and the total heating rate becomes proportional to the electron-grain recombination rate.

The calculated heating rate for the ISM is quite comparable to the heating rate derived from UV absorption studies of the level populations of the dominant cooling line, the [C II] 158 μm (Pottasch, Wesselius, & van Duinen 1979; Grey, Lequeux, & Boulanger 1993). In particular, for the well studied lines of sight toward ζ Oph, the observed cooling rate is 10^{-25} ergs s^{-1} (H atom)$^{-1}$. Using an incident intensity of the UV field $G_0 = 5$ (in Habing units) determined for this cloud (van Dishoeck & Black 1986), we calculate a photoelectric heating rate of 1.5×10^{-25} ergs s^{-1} (H atom)$^{-1}$; in good agreement with the observations.

Bock et al. (1993) directly measured the intensity of the C II line from the diffuse ISM at high galactic latitude. Their

observed heating rate of 2.5×10^{-26} ergs s^{-1} (H atom)$^{-1}$ is in good agreement with the value derived by Savage et al. (1993) from the C II UV absorption line toward 3C 273. The latter line of sight samples low-density gas ($n_{\rm H} \simeq 0.05$ cm^{-3}; see Savage et al. 1993), as expected for high latitudes. For this density, we calculate a heating rate of $\simeq 1.5 \times 10^{-26}$ ergs s^{-1} (H atom)$^{-1}$, assuming an electron fraction of 0.01 and a temperature of 50 K. For temperatures more in line with the warm neutral medium, our calculated value drops to $\simeq 3 \times 10^{-27}$ ergs cm^{-2} s^{-1} (H atom)$^{-1}$. We attribute the much lower heating rate of the ISM measured directly by Bock et al. (1993) as compared to the indirect measurement by Pottasch et al. (1979) to the difference in incident UV field coupled with the much lower density in the halo.

The FIRAS experiment on COBE has measured the total cooling rate of the galaxy in the [C II] 158 μm line (Wright et al. 1991). Combining this with the total dust emission measured also by COBE, we derive a heating efficiency of 0.003. The measured FIR continuum intensity of 5.9×10^{-3} ergs cm^{-2} s^{-1} sr^{-1} corresponds to a G_0 of $\simeq 50$. Adopting a typical diffuse cloud density of 30 cm^{-3} and a temperature of 100 K, we estimate an average heating efficiency of 0.003. The agreement with the observations is fortuitously good.

Figure 13 compares our photoelectric efficiencies with the semiempirical formalism of de Jong (1977). de Jong adopted the observed heating rate for diffuse interstellar clouds and ascribed it to neutral grains. Then, using a simple model for the charge of a (100 Å) grain, he derived the curve shown in Figure 13. Since our (ab initio) model also reproduces the observed heating rate of interstellar clouds well, the two models are in reasonable agreement for neutral grains (Fig. 13). However, since de Jong concentrated on relatively large grains, he overestimated the charging effect considerably. As a result for large $G_0 T^{1/2}/n_e$ (highly charged grains), his photoelectric heating rate decreases faster than ours. We now know that the interstellar grain size distribution extends well into the molecular domain (see Tielens 1990) and, hence, we believe that our formalism describes the photoelectric heating of the interstellar gas more accurately.

5.2. The Heating of PDRs

Over the last decade, many studies have been made both observationally and theoretically, of dense gas close to bright
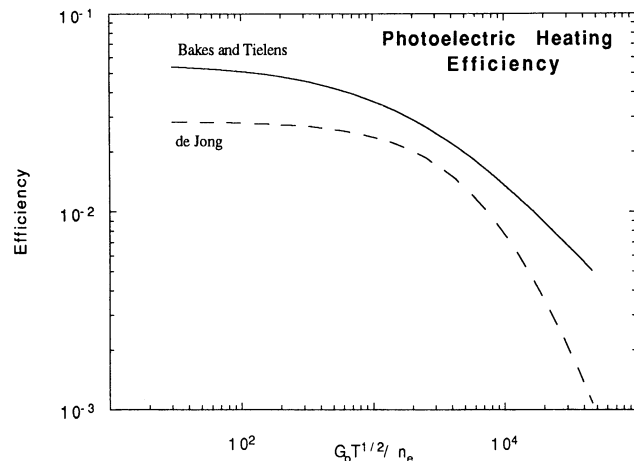

FIG. 13.—A comparison of our ab initio photoelectric efficiencies with the semiempirical formalism of de Jong (1977).

O and B stars (see the review by Genzel, Harris, & Stutzki 1989). These models and the analysis of these observations are built upon the de Jong formalism for the photoelectric effect. It is therefore of particular interest to consider the effects of our new photoelectric heating formalism on such models and observations. We have selected to rerun the standard model in Tielens & Hollenbach (1985), which is appropriate for the Orion PDR (see Table 2). The results of this calculation are shown in Figure 14 and described below.

The temperature profiles in the two formalisms are quite different (Fig. 14). In the TH85 model, the surface temperature is about 500 K and rises to a peak of about 1000 K. Essentially, in this model, the grains are highly positively charged at the surface, and the heating is much depressed. With increasing attenuation of the UV field into the slab, the average grain charge decreases, and, hence, the efficiency decreases. As a result, although the photoelectric heating rate decreases with depth into the cloud, the slowly decreasing heating rate is more than offset by the rapid decrease in the cooling rate due to optical depth effects in the dominant cooling line ([O I] 63 μm). Hence, the temperature increases somewhat until the grains are largely neutral, and the photoelectric efficiency does not increase anymore. In the new model, the gas reaches a higher temperature (~ 3000 K) at the surface due to the increased photoelectric efficiency for charged grains. The increase in photoelectric efficiency with depth into the slab (i.e., decreasing charge) plays less of a role now, and the temperature distribution remains quite constant. Eventually, the temperature drops because of dust attenuation of the heating UV photons. At depth $A_v \geq 2$, grains are neutral in both formalisms, and the temperature profiles converge. It should be emphasized that the total heating rate in our new models is only slightly larger than in the TH85 model. However, the cooling rate is very insensitive to temperature in this regime ($T \geq 228$ K, the excitation energy of the dominant cooling line), and, hence, this small increase in heating rate has a dramatic effect on the temperature. Other observables, such as the total gas cooling rate (i.e., the [O I] 63 μm intensity)—in fact, all FIR fine-structure lines—are much less affected. Thence, previous

analyses of observations (see Wolfire et al. 1990) of such lines are still reasonable, overestimating the derived densities by about a factor of 2.

6. RECOMBINATION COOLING

We have calculated the cooling, Λ, associated with electron recombination for a variety of physical conditions. The results are shown in Figure 15. The cooling depends of course on the recombination rate, which is proportional to the product $n_e n_H$. Hence, we have elected to show $\Lambda/n_e n_H$. The cooling rate increases with increasing $G_0 T^{1/2}/n_e$ due to the increase in the charge and thus in the Coulomb interaction. The cooling also increases with increasing gas temperature, since each recombination returns more energy to the grain. These trends in the recombination cooling are readily apparent in Figure 15. A simple analytical function can be derived which describes the essential features of the cooling. The cooling rate, $C(N_C, Z)$, by a species with N_C C atoms and charge Z is given by equation (31). For an attractive potential at low temperatures ($T \ll Ze^2/ak$), this reduces to $5.8 \times 10^{-21} n_e T^{1/2} N_C^{1/3} Z$ ergs s^{-1} (grain)$^{-1}$. The total cooling, Λ, is now the sum over all ionization stages and is then integrated over the size distribution. Replacing Z by the average charge $\langle Z \rangle$ for which we adopt $3 \times 10^{-3} N_C (G_0 T^{1/2}/n_e)^{0.4}$ from our numerical results, we find $d\Lambda/dN_C = 2.1 \times 10^{-29} n_e T^{1/2}(G_0 T^{1/2}/n_e)^{0.4} N_C^{-1.1}$. Detailed examination of our numerical results show a reasonable agreement with this simpleminded formula. The total cooling is now given by $10^{-28} n_e T^{1/2}(G_0 T^{1/2}/n_e)^{0.4}$ ergs s^{-1} (H atom)$^{-1}$. Actually, this underestimates the cooling at high temperatures ($\sim 10^4$ K) by a factor 3, mainly because at these temperatures Coulomb interaction is no longer as dominant. An analytical fit to our numerical results yields

$$\Lambda = 3.49 \times 10^{-30} T^\alpha (G_0 T^{1/2}/n_e)^\beta n_e n_H \quad \text{ergs}^{-1} \text{ cm}^{-3} , \quad (44)$$

where α is 0.944 and β is $0.735/T^{0.068}$. This fit is compared to the numerical data in Figure 15. Recombination cooling is particularly important for the warm intercloud medium. In Figure 16 we compare the recombination cooling rate of this phase with the photoelectric heating rate. At low temperatures,
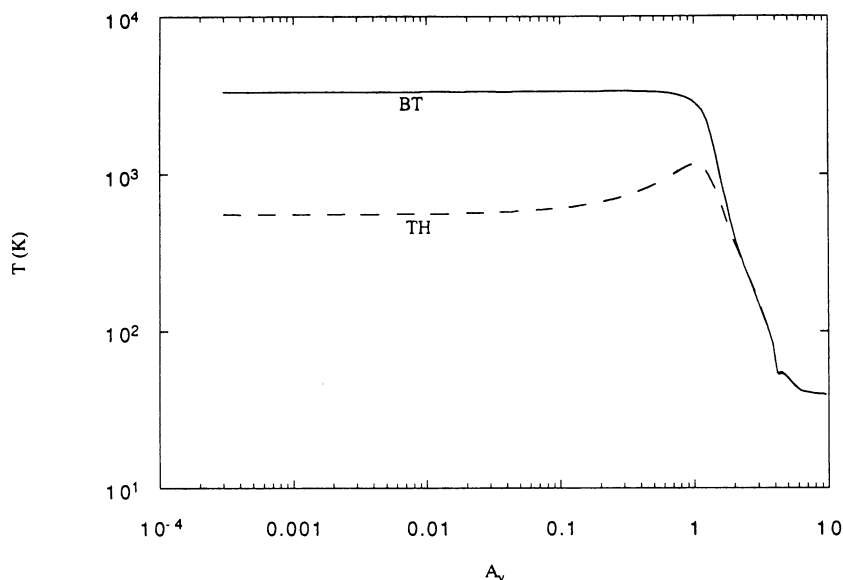

Fig. 14.—A comparison between the TH85 PDR model gas temperature profile and that formulated in this paper. See text for details.
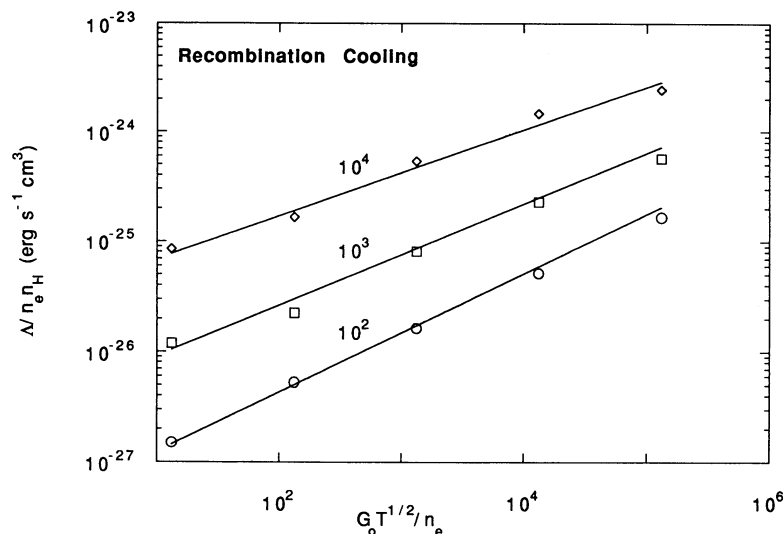
FIG. 15.—The recombination cooling for three different gas temperatures. The numerical evaluations are represented by points, while the lines represent analytic fits to these points.

the photoelectric effect dominates, while at high temperatures cooling is more efficient. Heating and cooling balance at about 15,000 K. The recombination cooling acts as a thermostat keeping the temperature below ~ 104 K.

The exact value of the temperature in the warm intercloud medium does depend somewhat sensitively on the absolute value of the heating rate. As illustrated in Figure 16, heating and cooling rates have very similar dependences on the physical conditions, and a small uncertainty in either rate can make a large difference in the resulting temperature.

7. SUMMARY

We have theoretically modeled the gas heating associated with the photoelectric ejection of electrons from PAHs and PAH clusters. We have considered a grain size distribution and included a charge distribution for each grain size. We have derived a simple analytical expression for the ionization rate and heating rate by grains of given size as a function of ionization potential. The charge balance has then been solved for various relevant physical conditions in the ISM. The resulting

grain charge distribution functions have been used to derive the total photoelectric heating rate for these conditions. We point out that small PAHs are likely to be negatively charged under typical conditions for the diffuse ISM. Table 3 summarizes the most probable charge for a grain of radius 5 and 100 Å and gives the average charge of the whole population in certain types of ISM. The results show that about half of the photoelectric heating is contributed by species with less than 1500 C atoms ($a = 15$ Å). The other half comes from grains with 1500–4.5×10^5 C atoms (15–100 Å). Although larger grains absorb about half of the available UV photon energy, they do not contribute appreciably to the photoelectric heating. This strong dependence of the heating on grain size largely reflects the shift in the charge balance with grain size. Essentially, the ionization over recombination rate scales with $N_C^{2/3}$, because the UV absorption cross section is proportional to the total number of C atoms, but the recombination scales with $N_C^{1/3}$ (Coulomb focusing). Hence, larger grains are more charged up and therefore contribute less to the heating.

We have considered a wide range of interstellar media ($1 < G_0 < 10^5$; $2.5 \times 10^{-3} < n_e < 75$; $10 < T < 10,000$ K) and derived the photoelectric heating efficiency (Fig. 11). The numerical results for this efficiency are well represented by a simple analytical expression (eq. [41]). The derived maximum efficiency (0.03) for neutral grains and the dependence on physical conditions is in good agreement with that expected from simple considerations. We have examined the effects of various parameters, including the electron escape length and the grain size distribution. As expected, the latter has a major effect on the total heating rate.
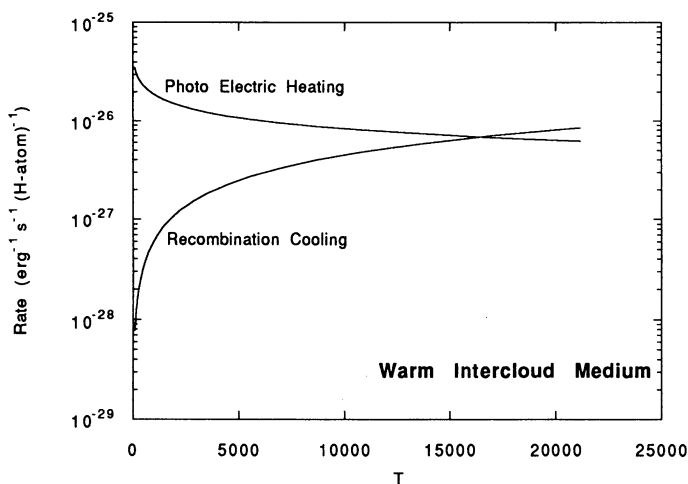
FIG. 16.—The numerical evaluation for the warm intercloud medium of recombination cooling and photoelectric heating.

TABLE 3
SUMMARY OF GRAIN CHARGING IN VARIOUS ISM

Environment	Z(5 Å) (disk)	Z(100 Å) (sphere)	⟨Z⟩
TH85 standard PDR model	0	+44	+
Cold diffuse ISM	0	+9	−, +
Warm ISM	0	+42	−, +

NOTES.—The sign of the average charge for each end of the grain size range is shown in the last column.

The calculated heating rates are in good agreement with the observations of the cooling rate of interstellar gas; both from UV absorption measurements of the populations of the fine structure levels of [C II] as well as with the direct IR measurements of the Galactic emission in this dominant cooling line. We have calculated the effects of the derived photoelectric heating rate on the temperature structure of the PDR associated with the Orion H II region. Finally, we describe the recombination cooling mechanism quantitatively as a function of the gas temperature, FUV flux, and electron and hydrogen nucleus density. We conclude that recombination cooling is most effi-cient at high gas temperatures and keeps the temperature of the warm intercloud medium below $\sim 10^4$ K.

REFERENCES

Allamandola, L. J., Tielens, A. G. G. M., & Barker, J. R. 1989, ApJS, 71, 733
Bock, J. J., et al. 1993, ApJ, 410, L115
Brus, L. E. 1983, J. Chem. Phys., 79, 5566
Christophorou, L. G., McCorkle, D. L., & Christodoulides, L. 1984, in Electron-Molecule Interactions and Their Applications, Vol. 2, ed. L. J. Christophorou (New York: Academic), 424
Crawford, M. K., Tielens, A. G. G. M., & Allamandola, L. J. 1985, ApJ, 293, L45
de Jong, T. 1977, A&A, 55, 137
Draine, B. T. 1978, ApJS, 36, 595
Draine, B. T., & Lee, H. M. 1984, ApJ, 285, 89
Draine, B. T., & Sutin, B. 1987, ApJ, 320, 803
Ferrière, K. M., Zweibel, E. G., & Shull, J. M. 1988, ApJ, 332, 984
Feuerbacher, B., Willis, R. F., & Fitton, B. 1973, ApJ, 181, 101
Gallegos, E. J. 1968, J. Phys. Chem., 72, 3452
Genzel, R., Harris, A. I., & Stutzki, J. 1989 in IR Spectroscopy in Astronomy: Proceedings of the ESLAD Symposium, ed. B. H. Kaldevich (ESA Publication Division)
Goldsmith, D. W., Habing, H. J., & Field, G. B. 1969, ApJ, 158, 173
Grey, C., Lequeux, J., & Boulanger, F. 1993, A&A, 266, 457
Habing, H. J. 1968, Bull. Astron. Inst. Netherlands, 19, 421
Hino, S., Sato, N., & Inokuchi, H. 1976, Chem. Phys. Lett., 37, 494
Hollenbach, D. J. 1989, in IAU Symp. 135, Interstellar Dust, ed. L. J. Allamandola & A. G. G. M. Tielens (Dordrecht: Kluwer), 227
Hollenbach, D. J., Takahashi, T., & Tielens, A. G. G. M. 1991, ApJ, 377, 192
Leach, S. 1987, in Polycyclic Aromatic Hydrocarbons in Astrophysics, ed. A. Léger, L. d'Hendecourt, & N. Bocarra (Dordrecht: Reidel), 99
Léger, A., & d'Hendecourt, L. 1987, in Polycyclic Aromatic Hydrocarbons in Astrophysics, ed. A. Léger, L. d'Hendecourt, & N. Bocarra (Dordrecht: Reidel)

Léger, A., & Puget, J. L. 1984, A&A, 137, L5
Makov, G., Nitzan, A., & Brus, L. E. 1988, J. Chem. Phys., 88, 5076
Mathis, J. S., Rumpl, W., & Nordsieck, K. H. 1977, ApJ, 217, 425
McKee, C. F., & Ostriker, J. P. 1977, ApJ, 218, 148
Moskovitz, M. 1991, Ann. Rev. Phys. Chem., 42, 465
Pope, M., & Swinberg, O. E. 1982, Electronic Processing in Organic Crystals (Oxford: Clarendon Press), 1
Pottasch, S. R., Wesselius, P. R., & van Duinen, R. J. 1979, A&A, 74, L15
Savage, B. D., Lu, L., Weymann, R. J., Morris, S. L., & Gilliland, R. L. 1993, ApJ, 404, 124
Sellgren, K. 1984, ApJ, 245, 138
Smith, F. T. 1961, J. Chem. Phys., 34, 793
Sternberg, A., & Dalgarno, A. 1989, ApJ, 338, 197
Tielens, A. G. G. M. 1990, in Submillimetre Astronomy, ed. G. D. Watt & A. S. Webster (Dordrecht: Kluwer), 13
Tielens, A. G. G. M., Allamandola, L. J., & Barker, J. R. 1987, in Polycyclic Aromatic Hydrocarbons in Astrophysics, ed. A. Léger, L. d'Hendecourt, & N. Bocarra (Dordrecht: Reidel), p. 255
Tielens, A. G. G. M., & Hollenbach, D. J. 1985, ApJ, 291, 722
Tobita, S., Meinke, M., Illenberger, E., Christophorou, L. G., Baumgärtel, H., & Leach, S. 1992, Chem. Phys., 161, 501
van Dishoek, E. L., & Black, J. H. 1986, ApJ, 307, 332
Verstraete, L., Léger, A., d'Hendecourt, L., Dutuit, O., & Deforneau, D. 1990, A&A, 237, 436
Watson, W. D. 1972, ApJ, 176, 103
Wolfire, M. G., Tielens, A. G. G. M., & Hollenbach, D. J. 1990, ApJ, 358, 116
Wood, D. M. 1981, Phys. Rev. Lett., 46, 749
Wright, E. L., et al. 1991, ApJ, 381, 200